RESEARCH

Generation and Selection of Driver-Behavior-Based Transferable Motion Primitives

Haijie Guan, Boyang Wang*, Jiaming Wei, Yaomin Lu, Huiyan Chen and Jianwei Gong

*Correspondence:
wbythink@hotmail.com
School of Mechanical Engineering,
Beijing Institute of Technology,
Zhongguancun South Street,
100081 Beijing, China
Full list of author information is
available at the end of the article

Abstract

In order to achieve the integration of driver experience and heterogeneous vehicle platform characteristics in the motion planning algorithm, based on the driver-behavior-based transferable motion primitives, a general motion planning framework for offline generation and online selection of motion primitives (MPs) is proposed. The optimal control theory is applied to solve the boundary value problems in the process of generating MPs, where the driver behaviors and the vehicle motion characteristics are integrated into the optimization in the form of constraints. Moreover, this paper proposes a layered, unequal-weighted MPs selection framework and utilizes the combination of environmental constraints, nonholonomic vehicle constraints, trajectory smoothness, and collision risk as the single-step extension evaluation index. The library of MPs generated offline demonstrates that the proposed generation method realizes the effective expansion of the MP types and achieves the diverse generation of MPs with various velocity attributes and platform types. We also present how the MP selection algorithm utilizes the unique MP library to achieve the online extension of MP sequences. The results show that the proposed motion planning framework can not only improve the efficiency and rationality of the algorithm based on driving experience but also can transfer between heterogeneous vehicle platforms and highlight the unique motion characteristics of the platform.

Keywords: autonomous vehicle; motion planning; motion primitives; driver behavior; heterogeneous vehicle platform

Introduction

The ever-increasing advancement of unmanned vehicle technology, especially multi-vehicle cooperative technology, will significantly promote the development of future intelligent transportation systems and unmanned combat systems and will affect the future travel modes and combat patterns [1–3]. In the unmanned vehicle system framework, motion planning is one of the crucial components. Its main function is to generate a reference trajectory that satisfies the constraints of the environment and the vehicle itself [4–6]. How to build a unified motion planning algorithm for heterogeneous vehicle platforms and use the driving experience to guide and accelerate the completion of planning tasks is one of the fundamental tasks for the further development of unmanned vehicle motion planning algorithms. In both the motion planning algorithm and the driving behavior representation algorithm, the decomposition of complex motion into motion primitives (MPs) can effectively improve the efficiency of the algorithm [7–10].

The essence of MPs generation is to solve a set of Boundary Value Problems (BVPs), i.e., to generate a set of paths connecting different target states [11]. The difficulty in solving the above problems lies in the segmentation strategy of the state space and the form of the curve connecting start and end state. Graph search-based motion planning algorithms, such as the typical A* [12, 13], D* [14, 15], and state lattice [16, 17], divide the environment space into basic grids and then generate MPs based on center points, corner points, or edges. Aiming at the disadvantages of a grid-based MP generation method that cannot consider nonholonomic vehicle constraints, the hybrid A* algorithm completes the generation of MPs based on the vehicle kinematic model [7, 18]. Each primitive used in the hybrid A* algorithm is an arc generated with a fixed time scale and a fixed front wheel angle. The discrete optimization-based method uses the spline curves or polynomial curves to generate the MP candidate sets based on the offset points of the road centerline, which effectively limits the search space and improves the overall efficiency of the algorithm [19–21]. Also, some methods use numerical optimization to realize the generation of MPs while considering vehicle dynamic constraints [22–24]. Although the MPs generated by the above methods can meet the complex driving environment's needs, they failed to integrate the driver's behavior information into the MP generation algorithm. Besides, these methods generally lack the consideration of the difference and connection of the heterogeneous platform motion characteristics.

The quality of the final path generated by the motion planning algorithm depends not only on the quality of the MP itself but also on the rationality of the MP selection and connection [25]. The selection of MPs is the process of first considering the cost function represented by different constraints, secondly combining the cost according to a particular weight factor, and finally selecting the MP with the minimum cost [26]. The Dijkstra algorithm takes the shortest path as the extension cost of the MP [27]. The A* algorithm and its variants add heuristics based on the target state and Voronoi diagram to the original Dijkstra algorithm [28]. The sampling-based RRT path planning algorithm [29], on the one hand, takes the target point as a guide to the selection and extension of MPs. On the other hand, it randomly extends in any direction with a certain probability to achieve a comprehensive search of the accessible areas. The Discrete optimization-based method [19] utilizes the linear combination of the three extension cost values considering static obstacles, dynamic obstacles, and path smoothness as the basis for the selection of MPs. Although the MP mentioned above selection and extension method can achieve the generation of the desired driving trajectory, no attention is paid to the guiding role of the driver's experience.

The learning and generalization of the driving experience and characteristics have attracted the attention of many researchers in recent years [30–32]. Specific to the trajectory-level driving behavior research, Guo et al. researched the generation of human-like trajectories with the leader vehicle as an attractive force [33]. Although the above method can cope with complex dynamic environments, the learning object of its behavior is the guide vehicle, i.e., it is a follow-up human-like trajectory generation method. Regarding the representation of human-like trajectories that target the behavior of the ego vehicle, Schnelle et al. proposed a personalized trajectory optimization generation method in two scenes: lane change and double lane

change [34]. Besides, Zhao et al. also conducted a series of research work on the lane change scene. Firstly, they used the support vector machine algorithm to extract lane change primitives from the lane change trajectory data of surrounding vehicles [35,36]. Subsequently, using the principle of trajectory matching, the generated human-like lane change trajectory was integrated into the real-time motion planning system [37,38]. However, the above research has limitations in the application of scenes. It is often aimed at a specific scene, and there is no further study on how to combine multiple driving behaviors with the vehicle motion planning system in the general driving environment.

In this paper, for the two heterogeneous platforms of wheeled Ackerman-steering vehicle and tracked skid-steering vehicle, a unified vehicle motion differential constraint is proposed. In addition, five kinds of equality constraints for typical driving behaviors and inequality constraints for vehicle platform characteristics are set, and an offline optimization method for driver-behavior-based transferable motion primitive (DBTMP) generation is formed. Based on the unique MP library established for different vehicle platforms, the research on the selection of MPs is carried out under the hybrid A* algorithm framework. However, there are two significant differences in the construction of the selection framework due to the big difference between the offline generated DBTMP library and the online generated MP library used by the hybrid A* algorithm. Firstly, the DBTMP library generated offline is a collection of multiple MP sets containing the entire speed interval, so a hierarchical structure is applied to restrict the MP candidate set. Secondly, since each candidate set contains both behavior primitives and general primitives, different weight coefficients are applied to the above two types of primitives when selecting and evaluating a single extended MP. Finally, a motion planning algorithm based on the offline generation and online selection of the DBTMP library is proposed.

The main contributions of this paper are shown as follows:

- A unified motion planning algorithm framework is proposed to complete the motion planning tasks of heterogeneous platforms, achieving a balance between the general solution framework and the characteristics of heterogeneous vehicle platforms.
- An offline MP generation method combining discrete driving behaviors and vehicle kinematics model is proposed, and the guiding role of behavior primitives to the online selection layer of motion planning algorithm is highlighted.

The remains of the paper are organized as follows. Section 1 details the problems to be solved in this paper and explains the main parameters. Section 2 introduces the offline generation method of the MP library. Section 3 introduces the online selection framework of MPs. Section 4 demonstrates the unique MP libraries of two heterogeneous vehicle platforms and the results of motion planning in two typical scenes. Finally, the conclusion and future work are given in Section 5.

1 Problem Statement

The offline MP generation is to solve the optimization problem with driver behaviors $\boldsymbol{B}$ and platform motion characteristics as constraints and trajectory smoothness as the objective function g. The selection of MPs is first to select the MP set from the MP library based on the passable area and velocity connection, and then utilize the

cost function J as the evaluation index to choose the corresponding single extended MP from the MP set.

The definition and explanation of the main parameters used in this paper are as follows:

- $\boldsymbol{s}(t) = [x(t), y(t), \theta(t)]^{\mathrm{T}} \in \mathbb{R}^{3\times1}$ is the unified state parameter set of each heterogeneous platform at time t, where $x(t)$ and $y(t)$ are the coordinate position of the x-axis and y-axis, $\theta(t)$ is the course angle. The defined coordinate system is the geodetic coordinate system xoy.
- $\boldsymbol{u}(t) = [v_{\mathrm{x}}(t), v_{\mathrm{y}}(t), \omega_{\mathrm{z}}(t)]^{\mathrm{T}} \in \mathbb{R}^{3\times1}$ is the unified control variable set of each heterogeneous platform at time t, where $v_{\mathrm{x}}(t)$ and $v_{\mathrm{y}}(t)$ are the velocity of the platform along the x-axis and y-axis, and $\omega_{\mathrm{z}}(t)$ is the yaw rate around the z-axis. The defined coordinate system is the geodetic coordinate system xoy.
- $\boldsymbol{u}_{\mathrm{a}}(t) = [v_{\mathrm{w_x}}(t), \alpha(t)]^{\mathrm{T}} \in \mathbb{R}^{2\times1}$ is the unique control variable set of the wheeled Ackerman-steering vehicle at time t, where $v_{\mathrm{w_x}}(t)$ is the velocity of the rear axle along the $\mathrm{x_a}$-axis, and $\alpha(t)$ is the front wheel angle of the vehicle. The defined coordinate system is the vehicle body coordinate system $\mathrm{x_a oy_a}$.
- $\boldsymbol{u}_t(t) = [v_{\mathrm{l_x}}(t), v_{\mathrm{r_x}}(t)]^{\mathrm{T}} \in \mathbb{R}^{2\times1}$ is the unique control variable set of the tracked skid-steering vehicle at time t, where $v_{\mathrm{l_x}}(t)$ and $v_{\mathrm{r_x}}(t)$ are the velocity of the left and right tracks along the $\mathrm{x_t}$-axis. The defined coordinate system is the vehicle body coordinate system $\mathrm{x_t oy_t}$.
- $\boldsymbol{D} = \boldsymbol{D}_{\mathrm{s}} \cdot \boldsymbol{D}_{\mathrm{a/t}}$ represents the mapping relationship between platform state parameters and control variables, where $\boldsymbol{D}_{\mathrm{s}}$ is the correlation between the unified state parameter set $\boldsymbol{s}$ and control variable set $\boldsymbol{u}$. $\boldsymbol{D}_{\mathrm{a/t}}$ is the correlation between the $\boldsymbol{u}$ and the unique control variable set $\boldsymbol{u}_{\mathrm{a/t}}$.
- $\boldsymbol{B}=\{B_{\mathrm{SD}}, B_{\mathrm{LC}}, B_{\mathrm{UT}}, B_{\mathrm{RT}}, B_{\mathrm{TA}}\}$ are the defined five kinds of driving behavior constraints, which are straight driving behavior B_{SD}, lane changing behavior B_{LC}, U-shaped turn behavior B_{UT}, right-angle turn behavior B_{RT}, and turn around behavior B_{TA}.
- $\boldsymbol{U}$ is the inequality constraint condition set according to the platform motion limit. $\boldsymbol{U}_{\mathrm{a}}$ and $\boldsymbol{U}_{\mathrm{t}}$ are for wheeled Ackerman-steering vehicle and tracked skid-steering vehicle.
- $\boldsymbol{J}=\{J_{\mathrm{e}}, J_{\mathrm{n}}, J_{\mathrm{s}}, J_{\mathrm{c}}\}$ is the cost function when selecting a single MP, where J_{e} is the environmental constraint heuristic, J_{n} is the nonholonomic vehicle constraint heuristic, J_{s} is the evaluation function considering the smoothness of the curve, and J_{c} is the evaluation function considering the collision risk.

The method proposed in this paper is dedicated to solving the following two challenges: First, how to generate a MP library that can be transferred between heterogeneous platforms, considering the overall versatility and highlighting the specificity of the vehicle platform. Second, how to integrate driving behavior factors into the generation and selection algorithm of the MPs, and then realize the guidance of the driver's experience to the motion planning algorithm.

2 Generation of MP

The generation process of DBTMP Library is shown in Fig.1. The entire processing flow can be decomposed into two main components, namely the creation and solution of optimal control problems and the rotation transformation and velocity

expansion of a single MP cluster. Among them, the definition of the optimal control problem for the single MP generation is the core of the generation method. The specific form of the optimal control problem is as follows:

$$\begin{aligned} &\min_{\boldsymbol{u}_{\mathrm{a/t}}}: \quad g(\boldsymbol{s},\boldsymbol{u}) \\ &\text{subject to :} \\ &\quad \boldsymbol{s}(t)=\boldsymbol{B} \qquad t\in[t_1,t_{\mathrm{g}}] \\ &\quad \dot{\boldsymbol{s}}(t)=f(\boldsymbol{s}(t),\boldsymbol{u}(t)) \qquad t\in[t_1,t_{\mathrm{g}}] \\ &\quad \boldsymbol{U}(t)\in\boldsymbol{U} \qquad t\in[t_1,t_{\mathrm{g}}] \end{aligned} \tag{1}$$

where $g(\boldsymbol{s},\boldsymbol{u})$ is the objective function of trajectory smoothness optimization based on the state parameters and control variables. $\boldsymbol{s}(t)=\boldsymbol{B}$ is the constraint condition of vehicle state based on driving behavior. $\dot{\boldsymbol{s}}(t)=f(\boldsymbol{s}(t),\boldsymbol{u}(t))$ is the motion differential constraint describing the relationship between the control variables and state parameters of the vehicle platform. $\boldsymbol{U}(t)\in\boldsymbol{U}$ is the inequality constraint condition set. t_1 and t_{g} are the start time and end time of MP generation respectively.

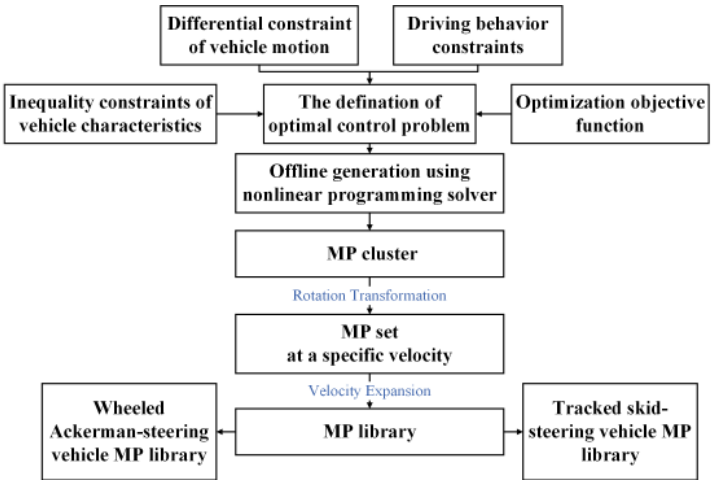

Figure 1 The DBTMP offline generation algorithm flow.

2.1 Vehicle Motion Differential Constraint

This paper ignores the impact of the suspension system on the vehicle motion response and regards the vehicle platform as a rigid body moving in a two-dimensional plane. The relationship between the unified state parameter set $\boldsymbol{s}$ and the unified control variable set $\boldsymbol{u}$ in the two-dimensional space is shown in Equation 2.

$$\begin{aligned} \dot{\boldsymbol{s}}(t) &= \boldsymbol{D}_{\mathrm{s}}\cdot\boldsymbol{u}(t) \\ &= \begin{bmatrix} \cos\theta(t) & -\sin\theta(t) & 0 \\ \sin\theta(t) & \cos\theta(t) & 0 \\ 0 & 0 & 1 \end{bmatrix} \begin{bmatrix} v_{\mathrm{x}}(t) \\ v_{\mathrm{y}}(t) \\ \omega_{\mathrm{z}}(t) \end{bmatrix} \end{aligned} \tag{2}$$

According to the characteristics of heterogeneous platform actuators, the mapping relationship between the unique control variable set $\boldsymbol{u}_{\mathrm{a/t}}$ and unified control variable

set $\boldsymbol{u}$ of different types of platforms is established, as shown in Equation 3.

$$\boldsymbol{u}(t) = \boldsymbol{D}_{\mathrm{a/t}} \cdot \boldsymbol{u}_{\mathrm{a/t}}(t) \tag{3}$$

The relationship between the control variable $\boldsymbol{u}_{\mathrm{a}}$ of a typical wheeled Ackerman-steering vehicle and the unified state parameter set $\boldsymbol{s}$ is shown in Equation 4, where L is the distance between the front and rear axis of the vehicle. The related coordinate system and a simplified model of the wheeled vehicle platform are shown in Fig.2.

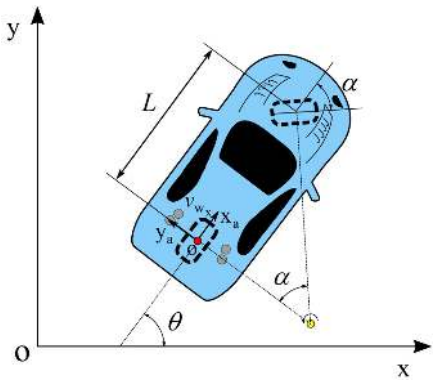

Figure 2 Wheeled Ackerman-steering vehicle.

$$\dot{\boldsymbol{s}}(t) = \boldsymbol{D}_{\mathrm{s}} \cdot \boldsymbol{D}_{\mathrm{a}} \cdot \boldsymbol{u}_{\mathrm{a}}(t) = \begin{bmatrix} v_{\mathrm{w_x}}(t)\cos\theta(t) \\ v_{\mathrm{w_x}}(t)\sin\theta(t) \\ v_{\mathrm{w_x}}(t)\tan\alpha(t)/\mathrm{L} \end{bmatrix} \tag{4}$$

The relationship between the control variable $\boldsymbol{u}_{\mathrm{t}}$ of a typical tracked vehicle and the unified state parameter set $\boldsymbol{s}$ is shown in Equation 5, where B is the distance between the two tracks. The related coordinate system and a simplified model of the tracked vehicle platform are shown in Fig.3.

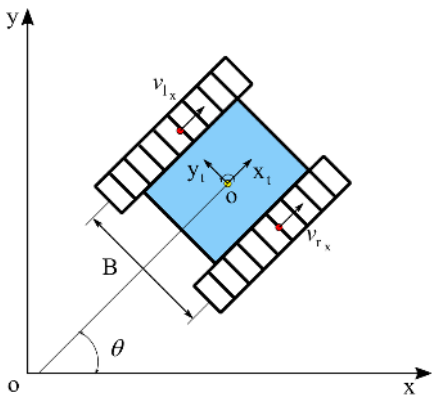

Figure 3 Tracked skid-steering vehicle.

$$\begin{aligned}\dot{\boldsymbol{s}}(t) &= \boldsymbol{D}_{\mathrm{s}} \cdot \boldsymbol{D}_{\mathrm{t}} \cdot \boldsymbol{u}_{\mathrm{t}}(t) \\ &= \begin{bmatrix} (v_{\mathrm{l_x}}(t) + v_{\mathrm{r_x}}(t)) \cos\theta(t)/2 \\ (v_{\mathrm{l_x}}(t) + v_{\mathrm{r_x}}(t)) \sin\theta(t)/2 \\ (v_{\mathrm{r_x}}(t) - v_{\mathrm{l_x}}(t))/2\mathrm{B} \end{bmatrix}\end{aligned} \tag{5}$$

2.2 Equality Constraints of Driving Behavior

This paper defines five typical driving behaviors, as shown in Fig.4. These typical behaviors include B_{SD} and B_{LC} that exist throughout the velocity range, as well as B_{UT}, B_{RT}, and B_{TA} that exist only in the low velocity range. Due to the specificity of the vehicle structure, B_{TA} can be subdivided into $B_{\mathrm{TA_a}}$ for wheeled vehicle and $B_{\mathrm{TA_t}}$ for tracked vehicle.

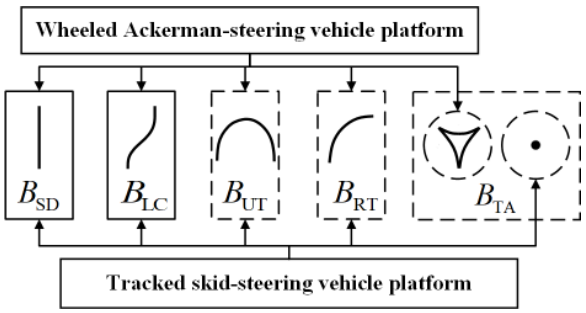

Figure 4 Driver behavior MPs.

For straight driving behavior B_{SD}, U-shaped turn behavior B_{UT} and right-angle turn behavior B_{RT}, only the course angle change between the start state t_1 and the end state t_{g} is constrained.

$$B_{\mathrm{SD}} = \theta(t_{\mathrm{g}}) - \theta(t_1) = 0 \tag{6}$$

$$B_{\mathrm{UT}} = \theta(t_{\mathrm{g}}) - \theta(t_1) = \pi \tag{7}$$

$$B_{\mathrm{RT}} = \theta(t_{\mathrm{g}}) - \theta(t_1) = \pi/2 \tag{8}$$

For lane changing behavior B_{LC}, in addition to restraining the course angle change deviation, the lateral distance change deviation d should also be constrained.

$$B_{\mathrm{LC}} = \begin{bmatrix} \theta(t_{\mathrm{g}}) - \theta(t_1) \\ [\cos\theta(t_{\mathrm{g}}), \sin\theta(t_{\mathrm{g}})][x(t_{\mathrm{g}}), y(t_{\mathrm{g}})]^{\mathrm{T}} - d \end{bmatrix} = 0 \tag{9}$$

For turn around behavior $B_{\mathrm{TA_a}}$ of wheeled vehicle, it is necessary not only to restrict the beginning and end states but also to restrict the intermediate states accordingly.

$$B_{\mathrm{TA_a}} = \begin{bmatrix} \theta(t_{\mathrm{g}}/3) - \theta(t_1) - \pi/3 \\ \theta(2t_{\mathrm{g}}/3) - \theta(t_{\mathrm{g}}/3) + 2\pi/3 \\ \theta(t_{\mathrm{g}}) - \theta(2t_{\mathrm{g}}/3) - \pi/3 \end{bmatrix} = 0 \tag{10}$$

Since the tracked vehicle can complete the task of turn around through the pivot turn movement, its constraint relationship B_{TAt} is as follows:

$$B_{\mathrm{TA_t}} = \begin{bmatrix} x(t_\mathrm{g}) - x(t_1) \\ y(t_\mathrm{g}) - y(t_1) \\ \theta(t_\mathrm{g}) - \theta(t_1) - \pi \end{bmatrix} = 0 \tag{11}$$

2.3 Inequality Constraints of Vehicle Platform Characteristics

The constraints of vehicle platform characteristics mainly include four aspects: the input range of control variable $\boldsymbol{u}$, the limitation of yaw rate ω_z, the limitation of lateral acceleration a_y, and the limitation of the current generated MP velocity attribute v.

$$\boldsymbol{U} = \begin{Bmatrix} \boldsymbol{u} \in [-\boldsymbol{u}_{\max}, \boldsymbol{u}_{\max}] \\ \omega_\mathrm{z} \le 0.8 \\ a_\mathrm{y} \le 0.4\mathrm{g} \\ v \in [v_{\mathrm{low}}, v_{\mathrm{up}}] \end{Bmatrix} \tag{12}$$

The inequality constraint relationship $\boldsymbol{U}_\mathrm{a}$ of wheeled Ackerman-steering vehicle is shown in Equation 13, where $\alpha_{\max}$ is the maximum front wheel angle of the vehicle platform.

$$\boldsymbol{U}_\mathrm{a} = \begin{Bmatrix} \alpha \in [-\alpha_{\max}, \alpha_{\max}] \\ v_{\mathrm{w_x}} \tan\alpha / \mathrm{L} \le 0.8 \\ v_{\mathrm{w_x}}^2 \tan\alpha / \mathrm{L} \le 0.4\mathrm{g} \\ v_{\mathrm{w_x}} \in [v_{\mathrm{low}}, v_{\mathrm{up}}] \end{Bmatrix} \tag{13}$$

The inequality constraint relationship U_t of tracked skid-steering vehicle is shown in Equation 14, where $v_{\mathrm{l_x\_max}}$ and $v_{\mathrm{r_x\_max}}$ are the maximum speed limits of the left and right driving wheels respectively.

$$\boldsymbol{U}_\mathrm{t} = \begin{Bmatrix} v_{\mathrm{l_x}} \in [-v_{\mathrm{l_x\_max}}, v_{\mathrm{l_x\_max}}] \\ v_{\mathrm{r_x}} \in [-v_{\mathrm{r_x\_max}}, v_{\mathrm{r_x\_max}}] \\ 2\left|v_{\mathrm{l_x}} - v_{\mathrm{r_x}}\right| / \mathrm{B} \le 0.8 \\ \left|v_{\mathrm{l_x}}^2 - v_{\mathrm{r_x}}^2\right| / 2\mathrm{B} \le 0.4\mathrm{g} \\ (v_{\mathrm{l_x}} + v_{\mathrm{r_x}})/2 \in [v_{\mathrm{low}}, v_{\mathrm{up}}] \end{Bmatrix} \tag{14}$$

2.4 Objective Function and Optimization Problem Solving

The objective function mainly reflects the requirements for the smoothness of the generated MPs. The objective function g_a for the wheeled Ackerman-steering platform is shown in Equation 15, and the objective function g_t for the tracked skid-steering vehicle platform is shown in Equation 16.

$$g_\mathrm{a} = \int_0^{t_\mathrm{g}} (\alpha(t)^2 + v_{\mathrm{w_x}}(t) \frac{\tan\alpha(t)}{\mathrm{L}}) dt \tag{15}$$

$$g_\mathrm{t} = \int_0^{t_\mathrm{g}} (\frac{(v_{\mathrm{l_x}}(t) + v_{\mathrm{r_x}}(t)}{2})^2 + \frac{2(v_{\mathrm{l_x}}(t) - v_{\mathrm{r_x}}(t))}{\mathrm{B}}) dt \tag{16}$$

In this paper, the IPOPT [39] and CVODES [40] are applied to solve the optimal control problem.

2.5 Generation of MP Library

Due to the complexity of the real driving environment, only the defined driving behavior MPs cannot fully satisfy the motion planning problem in a complex environment. Therefore, in order to improve the applicability of the MP library, the general MPs are generated as a supplement with the target course angle uniformly distributed on $[0, 2\pi]$ as the constraint.

After generating the MP cluster containing behavior primitives and general primitives, a MP set covering the entire annular space with 36 MP clusters evenly distributed is generated by rotation transformation. A simplified schematic diagram of the MP set generation is shown in Fig.5, and only a part of typical MPs and the rotation transformation at three positions are shown in the figure. The resulting MP library is a combination of multiple MP sets under different MP velocity attribute settings.

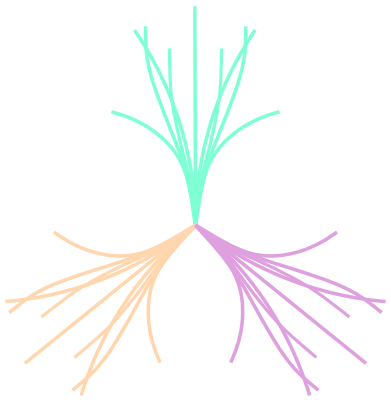

Figure 5 MP cluster rotation transformation.

3 Selection of MP

The selection process of MP is shown in Fig.6. The entire processing flow can be decomposed into the selection of the MP sets, the calculation of heuristics and costs, the selection of a single MP, and the extension of the MP sequence. The selection of MP sets refers to selecting the appropriate MP sets from the MP library based on passable areas in the environment map and velocity attribute of the last extended periodic MP set. The heuristics include both environmental constraint heuristic and nonholonomic vehicle constraint heuristic. The environmental constraint heuristic is calculated from the starting and target poses in the grid map. The nonholonomic vehicle constraint heuristic is calculated based on the final state of every single MP in the MP set and the target pose set by the planning system. The extension costs include the trajectory smoothing cost represented by the curve energy and the collision risk cost characterized by the distance from the obstacle. Finally, the linear combination of heuristics and costs is selected as the basis for single-step MP extension, and the selected multiple MPs are combined into a MP sequence to complete the motion planning task.

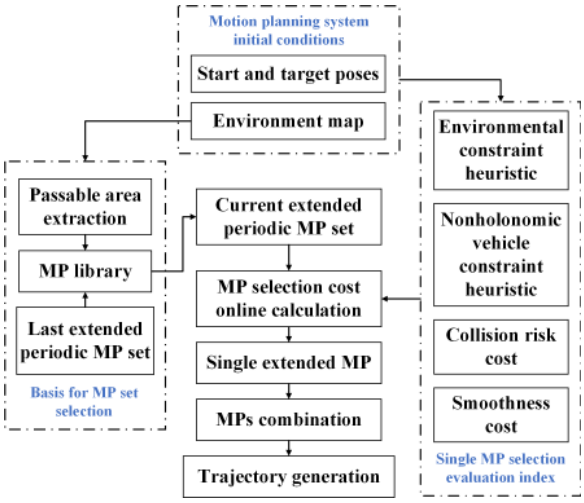

Figure 6 The DBTMP online selection algorithm flow.

3.1 Selection of MP Sets

The extraction of the single-step extended passable area is shown in Fig.7. The radius of the passable area r_{area} is calculated by the closest distance $d_{\min} = \min\{d_{\text{obs\_1}}, d_{\text{obs\_2}}, ..., d_{\text{obs\_n}}\}$ between the current position and the obstacle. The candidate set of MPs need to satisfy the essential condition that the final state of every single MP is within the passable area.

In addition, considering the velocity attribute association of two adjacent periodic MPs, the MP set with a large velocity gap from the previous periodic is eliminated from the candidate set. Finally, the further narrowing of the candidate set is achieved.

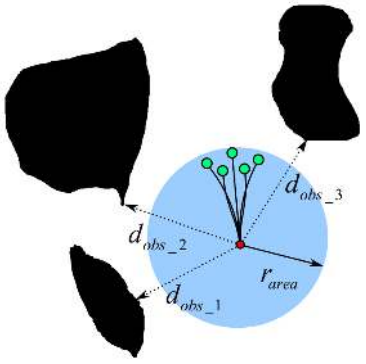

Figure 7 Single-step extended passable area extraction.

3.2 Heuristics Considering Environmental and Nonholonomic Constraints

The calculation of the environmental constraint heuristic J_{e} takes the target position as the initial point and utilizes the breadth-first-search algorithm to realize the

iterative expansion of the distance cost until it expands to the starting position. The specific algorithm flow is shown in Algorithm 1.

Algorithm 1 Pseudocode for computing environmental constraint heuristic

Require: starting point n_{start}; target point n_{goal}; open list S_{open}; heuristic value $J_{\text{e}}(n)$; iteration value ΔJ

$S_{\text{open}} \leftarrow \{n_{\text{goal}}\}$
$\{J_{\text{e}}(n_1), J_{\text{e}}(n_2) \cdots J_{\text{e}}(n_{\text{all}})\} \leftarrow \infty, J_{\text{e}}(n_{\text{goal}}) \leftarrow 0$
while $\emptyset \neq S_{\text{open}}$ **do**
  $n \leftarrow \text{Pop}(S_{\text{open}})$ {select the grid with the smallest heuristic value in open list}
  $\text{ExpandNode}(n, n_{\text{new}})$ {take the current grid as the center grid and expand in the direction of the surrounding eight grids}
  if $(\text{CollisionCheck}(n))$ **then**
    continue;
  else if $(n_{\text{new}} == n_{\text{start}})$ **then**
    break;
  else
    $J_{\text{e}}(n_{\text{new}}) \leftarrow J_{\text{e}}(n) + \Delta J$ {heuristic value addition}
    $S_{\text{open}} \leftarrow \{n_{\text{new}}\}$
  end if
end while

Fig.8 shows the comparison results of the environmental constraint heuristics calculated based on the Euclidean distance and the breadth-first algorithm used in this paper. It can be found from Fig.8(a) that the calculated heuristics will first guide the MP to extend to the obstacle area, as shown by the dotted blue arrow in the figure. On the contrary, in Fig.8(b), the MP is guided to the passable area, as shown by the solid blue arrow in the figure. Therefore, the environmental constraint heuristic proposed in this paper can avoid invalid extended search and effectively improve the efficiency of the algorithm.

(a) Euclidean distance (b) Breadth first

Figure 8 Comparison of environmental constraint heuristics.

This paper also introduces the vehicle nonholonomic constraint heuristic J_{n} taking the length of the Reeds-Shepp curve as the heuristic value. The Reeds-Sheep curve is composed of a fixed curvature arc and a straight line. It can quickly generate a curve connecting the start and end points while meeting the position and course constraints of the two points. The nonholonomic constraint heuristic introduces the evaluation of the target point's course reachability under the premise of considering the vehicle's motion characteristics, which makes up for the defect that the environmental constraint heuristic only considers the target position's reachability.

Finally, the larger value of the environmental constraint heuristic and nonholonomic constraint heuristic is selected as the final heuristic value of the grid, i.e., $J_1 = \max\{J_e, J_n\}$.

3.3 Extension Costs Considering Smoothness and Collision

The extension cost proposed in this paper mainly includes two aspects: trajectory smoothness and possible collision risk.

The extension cost value of smoothness J_s is calculated using the curve energy function as shown in Equation 17, the essence of this function is the discrete representation of the curvature integral on the curve.

$$J_s = \sum_{i=2}^{N} \frac{(\kappa_{i-1}^2 + \kappa_i^2)\Delta s_i}{2} \tag{17}$$

where N is the number of discrete points of the curve, κ_i is the corresponding curvature of the point, and Δs_i is the distance between two adjacent points.

The extension cost value of collision risk J_c is calculated using the function shown in Equation 18, and the vehicle platform is approximated by the six coverage circles shown in Fig.9 during the calculation process.

$$J_c = \frac{\sum_{i=1}^{6} (d_{obs\_i} - r_i)}{6} \tag{18}$$

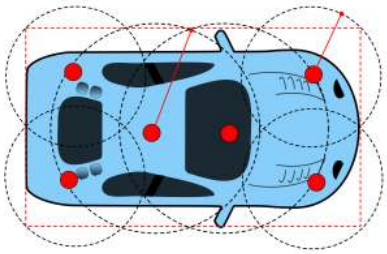

Figure 9 Six covered circles of vehicle platform.

where d_{obs_i} is the distance from the center of each coverage circle to the nearest obstacle, and r_i is the radius of each coverage circle.

The above extension costs J_s and J_c are given different weighting coefficients ω_s and ω_c. The linear combination after weighting is the final extension value as shown in Equation 19.

$$J_2 = \omega_s J_s + \omega_c J_c \tag{19}$$

The weighting coefficient ω_s is differentiated according to the types of MPs as shown in Equation 20. In principle, the relationship between the weight values of

behavior MPs ω_{s_B}, general MPs ω_{s_G} and MPs in reverse direction ω_{s_D} is: $\omega_{s_B} < \omega_{s_G} \ll \omega_{s_D}$.

$$\omega_s = \begin{cases} \omega_{s_B} & \text{if} \quad \text{mp}_i == \text{Behavior MP} \\ \omega_{s_G} & \text{if} \quad \text{mp}_i == \text{General MP} \\ \omega_{s_D} & \text{if} \quad \text{mp}_i == \text{Reverse Direction} \end{cases} \tag{20}$$

3.4 Evaluation Function of MP Selection

The total cost of selecting a single MP mp_i in the MP candidate set should be the sum of the corresponding heuristic and extension cost, as shown in Equation 21.

$$J(\text{mp}_i) = J_1(\text{mp}_i) + J_2(\text{mp}_i), \quad i \in [0, N_p] \tag{21}$$

where N_p is the number of independent MPs in the MP candidate set. In the extension process of MPs at each step, the MP with the smallest total cost in the MP candidate set is selected for an extension. Finally, the desired trajectory generation from the start position to the end position in the environment map is realized.

4 Experimental Results and Discussion

In order to verify the effect of the DBTMP A* motion planning algorithm proposed in this paper, the wheeled Ackerman-steering vehicle and tracked skid-steering vehicle were chosen respectively, and the corresponding tests were carried out in both the simulation environment and the real environment. In the simulation environment, we mainly conducted an in-depth comparative analysis of the algorithm performance in low-speed and high-speed scenes. In the real environment, we mainly focused on the applicability of the algorithm in real situations, especially the compatibility with the platform and the corresponding autonomous driving module. In addition, the classic Hybrid A* method was also selected as a comparison reference. The specific platform parameters are shown in Table 1, where P_a represents the wheeled Ackerman-steering platform and P_t represents the tracked skid-steering platform.

Table 1 Platform geometric parameters and actuator constraints.

Type	B (m)	L (m)	α_{max} (deg)	$v_{l_{x\text{-}max}}$ (m/s)	$v_{r_{x\text{-}max}}$ (m/s)
P_a	4.3	1.9	$\pi/6$	-	-
P_t	5.2	3.3	-	16	16

4.1 MP Library Offline Generation

The MP libraries for both platforms used a unified optimization framework during the generation process, and only the details of the vehicle characteristic constraints were changed during the platform transformation process.

The overall situation of the two platform MP libraries is shown in Table 2, where v_m(m/s) is the velocity attribute of the MP set, d_m(m) is the longest distance covered by the MP set, N_B is the number of behavior primitives in the MP set, N_m is the number of general primitives in the MP set, 36 is the number of MP clusters

after rotation transformation included in each MP set, $\bar{J}_{\mathrm{s}}$ is the average curve energy value of each MP in the set. At the end of Table 2, the overall situation of the MP library used by the Hybrid A* method which does not distinguish between vehicle platforms and velocity attributes is presented.

Table 2 The generated MP library. This table lists the composition structure of the DBTMP library generated offline for the wheeled Ackerman-steering platform and tracked skid-steering platform. The structure of the online generated MP library used by the Hybrid A* algorithm is also introduced as a comparison reference.

Platform	v_m	d_m	N_{B}	N_{m}	J_{s}
$\mathrm{P_a}$	5	20	16*36	49*36	0.0643
$\mathrm{P_a}$	10	25	23*36	20*36	0.1099
$\mathrm{P_a}$	12	30	25*36	20*36	0.1748
$\mathrm{P_a}$	14	35	25*36	20*36	0.1473
$\mathrm{P_a}$	16	40	25*36	20*36	0.1242
$\mathrm{P_a}$	18	40	9*36	8*36	0.1067
$\mathrm{P_a}$	22	40	9*36	6*36	0.0933
$\mathrm{P_a}$	26	40	9*36	6*36	0.0824
$\mathrm{P_a}$	30	40	9*36	6*36	0.0784
$\mathrm{P_t}$	5	15	18*36	64*36	1.3136
$\mathrm{P_t}$	10	25	23*36	20*36	0.2426
$\mathrm{P_t}$	12	30	25*36	20*36	0.1694
$\mathrm{P_t}$	14	35	9*36	8*36	0.1307
$\mathrm{P_t}$	16	40	9*36	8*36	0.1065
Hybrid	-	online adjustment	-	17*36	0.2095

In order to show the generated MP clusters more intuitively, Fig.10 presents low-speed and high-speed typical MP clusters with wheeled platform velocity attributes of 5m/s and 18m/s, and tracked platform velocity attributes of 5m/s and 16m/s. It also includes the MP cluster used by the Hybrid A* method.

The offline generation result of the MP library demonstrated that no matter what type of vehicle platform, the number of MPs gradually decreased with the increase of velocity. The reason is that the vehicle can achieve more diversified steering movements at low speeds, but the number of MPs at high speeds is greatly reduced due to the weakening of steering ability.

It can be observed from Table 2 that the average energy of the wheeled platform MPs in the low-speed range was lower than that of the tracked platform. On the one hand, it shows that the trajectory of the wheeled platform is smoother, and the adjustment of the course is gentler. On the other hand, it also indicates that the tracked platform has stronger and more aggressive steering adjustment ability at low speed. In the high-speed range, the MPs average energy of the two platforms was basically the same, and the steering adjustment tended to be the same.

Hybrid A* utilized a circular arc generated by a fixed curvature as the basic MP. It neither realized the differentiation of the characteristics of heterogeneous platforms nor the separation of different speed intervals. In general, the types of MPs are relatively limited and do not have the diversity of MPs in the DBTMP library proposed in this paper.

4.2 Comparative Analysis of MPs Online Selection in Simulation Environment

In order to demonstrate the performance of the MPs online selection algorithm proposed in this paper, a low-speed scene and a high-speed scene were designed to evaluate the motion planning algorithm. In each scene, the motion planning results of Hybrid A*, DBTMP A*-$\mathrm{P_a}$, and DBTMP A*-$\mathrm{P_t}$ were compared. The planning

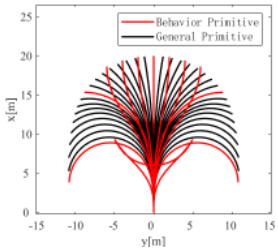

(a) 5m/s wheeled Ackerman-steering platform

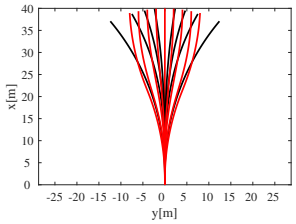

(b) 18m/s wheeled Ackerman-steering platform

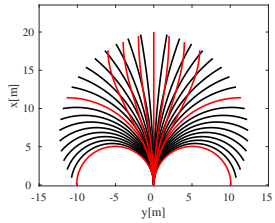

(c) 5m/s tracked skid-steering platform

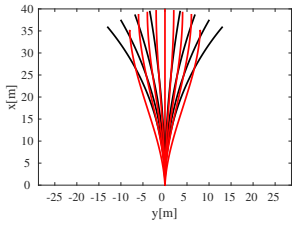

(d) 16m/s tracked skid-steering platform

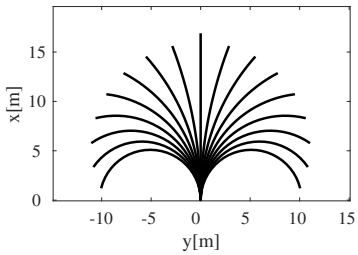

(e) Hybrid A*

Figure 10 Comparison of motion primitive cluster generation results.

results were solved by a laptop Lenovo-Ideapad Y700-15ISK with 16G memory, Intel Core i7-6700@2.6GHZ×8, running under Ubuntu 16.04 64bits. The entire motion planning algorithm was written in C++ in the ROS system.

Fig.11 shows the results of motion planning in low-speed scenes. Table 3 demonstrates the comparison results of the corresponding evaluation indicators, including the average curve energy $\bar{J}_{\mathrm{s}}$, the total number of MP extensions N_{e}, the number of behavior primitives during extension N_{be}, and the solution time of the corresponding motion planning algorithm T(ms).

Table 3 Comparison of MP online selection results in low-speed scene.

Method	J_{s}	$N_{\mathrm{be}}/N_{\mathrm{e}}$	T
Hybrid A*	1.9371	0/23	132.43
DBTMP A*-$\mathrm{P_a}$	0.0602	12/16	44.38
DBTMP A*-$\mathrm{P_t}$	0.0578	17/18	48.15

From the perspective of smoothness of the motion planning results, no matter which platform was used, the trajectory generated by the DBTMP A* algorithm is

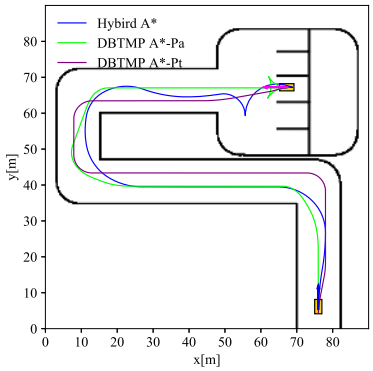

(a) Motion planning comparison results

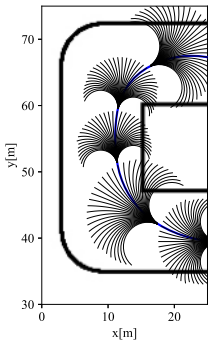

(b) Hybrid A* extension detail

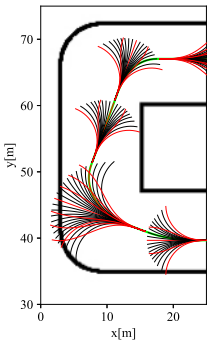

(c) DBTMP A*-P_a extension detail

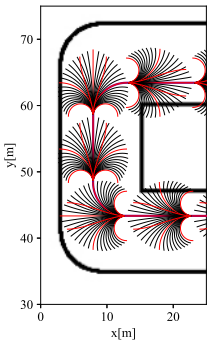

(d) DBTMP A*-P_t extension detail

Figure 11 Comparison of motion planning results in low-speed scenes. Firstly, under the same initial and final state conditions, the three motion-planning algorithms are compared, as shown in Fig.11(a). In Fig.11(a), the blue and purple arrow indicates the position and heading of the initial and end separately. The following sub-figures (Fig.11(b)-Fig.11(d)) respectively show the details of the MPs extension of the three motion planning methods. In the three detailed sub-figures, the final selected single MP in the MP cluster is represented by a thick solid line.

smoother. One of the reasons is that the overall MP library used by the DBTMP A* algorithm is smoother than the Hybrid A* method. Another reason is that the straight driving behavior primitives and general primitives use different weighting coefficients in the evaluation (as shown in Equation 20), so the straight driving behavior primitives occupy a larger proportion of the entire trajectory, which makes the evaluation index of smoothness significantly lower than Hybrid A* algorithm.

From the perspective of the extension times of MPs, the extension times of DBTMP A*-P_a and DBTMP A*-P_t were only 69.56% and 78.26% of the hybrid A* method. This is mainly because the introduction of behavior primitives makes the extension category of a single MP increase and improves the adaptability to the environment so that it can complete the trajectory planning task with fewer MP combinations. This was most evident in the local scene of the parking scene at the end. Regardless of the vehicle platform, the DBTMP A* algorithm used only one MP to complete the planning task, while the Hybrid A* achieved the task through the joining of 5 independent MPs and did not highlight the characteristics of the two platforms.

From the perspective of the solution time of motion planning tasks, the DBTMP A* algorithm only took up 35% of the overall solution time of the Hybrid A* algorithm. The main reason is that the MP sets used by the Hybrid A* algorithm are generated online based on the radius of the passable, while the MP sets selected by the DBTMP A* algorithm are generated offline.

The comparison results of motion planning in high-speed scenes are shown in Fig.12, and Table 4 demonstrates the corresponding evaluation indicators.

Table 4 Comparison of MP selection results in high-speed scene.

Method	J_s	N_{be}/N_e	T
Hybrid A*	0.0577	0/8	90.4616
DBTMP A*-P_a	0.0093	4/4	57.2816
DBTMP A*-P_t	0.0071	4/4	55.6434

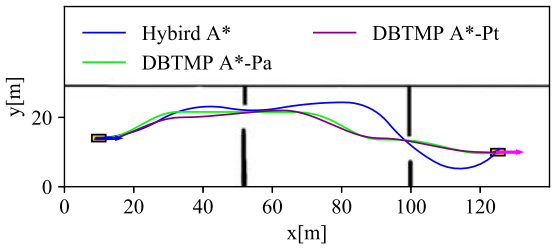

(a) Motion planning comparison results

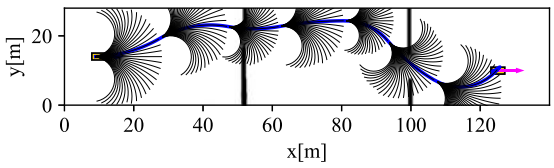

(b) Hybrid A* extension detail

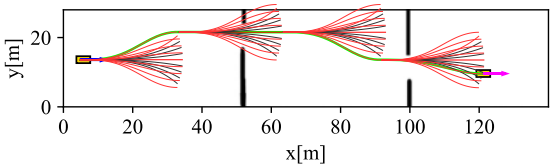

(c) DBTMP A*-P_a extension detail

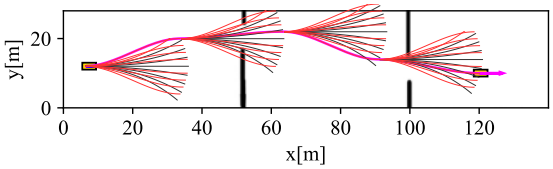

(d) DBTMP A*-P_t extension detail

Figure 12 Comparison of motion planning results in high-speed scenes.

From the motion planning results of Fig.12 and Table 4, the algorithm proposed in this paper took advantage of the DBTMP library to achieve lower curve energy, fewer extension times, shorter solution time and more reasonable planning result. This is mainly because the DBTMP library restricts and distinguishes the MPs that can be selected according to the velocity attribute and introduces the standard lane-change driving behavior primitives in high-speed scenes as supplements. This makes the driving experience successfully integrated into the MP generation and selection process proposed in this paper. Although the Hybrid A* algorithm can also plan the corresponding collision-free trajectory, it does not conform to the driver's driving experience in high-speed scenes.

4.3 Applicability of the Algorithm in Real Environment

The performance of the proposed algorithm in the real environment is verified by two vehicle platforms, namely the wheeled Ackerman-steering platform shown in Fig.13(a) and the tracked skid-steering platform shown in Fig.13(b). The two platforms are equipped with the same equipment, including a RoboSense 32-lidar and two RoboSense 16-lidars, a Simpak982 GNSS receiver, a FOSN2 inertial navigation system, an AVT-1290c camera, and two industrial personal computers.

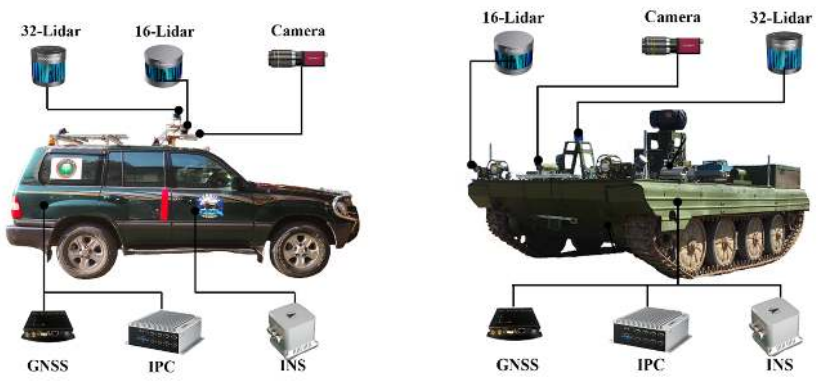

(a) Wheeled Ackerman-steering platform (b) Tracked skid-steering platform

Figure 13 Unmanned vehicle test platforms.

Before the experiment, we have obtained the environmental map required for the entire planning task through a multi-source SLAM algorithm. In the experiment, the fusion positioning system provided centimeter-level real-time positioning accuracy at a frequency of 50HZ. On the basis of a priori map, the environment perception equipment carried by the vehicle added real-time environmental information to the map at a frequency of 5HZ. Model predictive control was selected as the vehicle motion control algorithm, and the comprehensive tracking error in the off-road environment is less than 0.5m.

The purpose of the experiment in real scenes is mainly to test the performance and efficiency of the algorithm under complex environmental conditions. Fig.14 demonstrates the comparison results of the motion planning algorithm at two-time points during the unmanned driving. These two moments were the starting moment

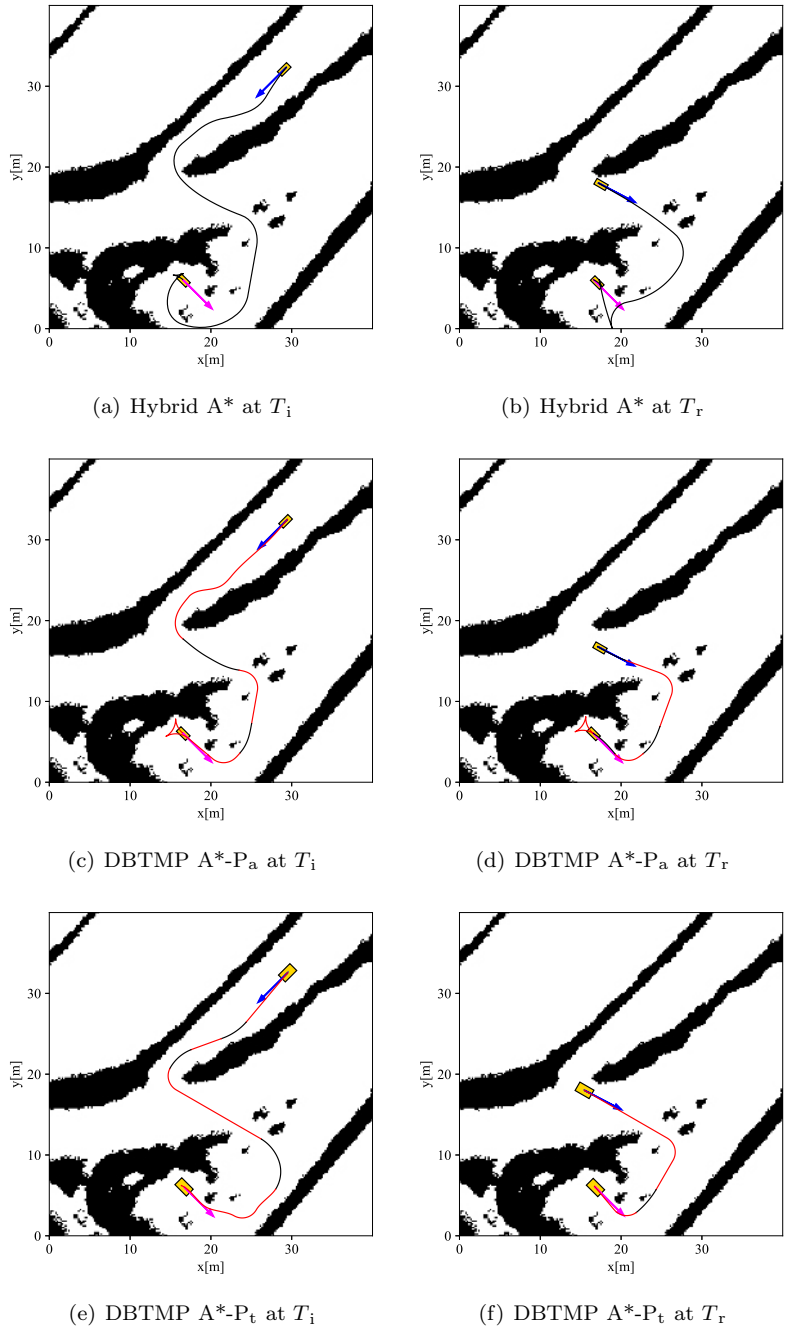

(a) Hybrid A* at T_{i} (b) Hybrid A* at T_{r}

(c) DBTMP A*-$\mathrm{P_a}$ at T_{i} (d) DBTMP A*-$\mathrm{P_a}$ at T_{r}

(e) DBTMP A*-$\mathrm{P_t}$ at T_{i} (f) DBTMP A*-$\mathrm{P_t}$ at T_{r}

Figure 14 Comparison results of three motion planning algorithms in real environments. The Hybrid A* algorithm only made extremely limited adaptability adjustments for the two platforms, so only the wheeled Ackerman-steering platform was selected as the verification platform. T_{i} represents the initial moment of the planning, and T_{r} represents the moment of replanning.

of planning and the trigger moment of replanning after turning. Fig.15 shows the efficiency indexes of the three motion planning algorithms.

Judging from the experimental results in real scenes, the algorithm proposed in this paper can not only be applied in unmanned systems in real-time but can also

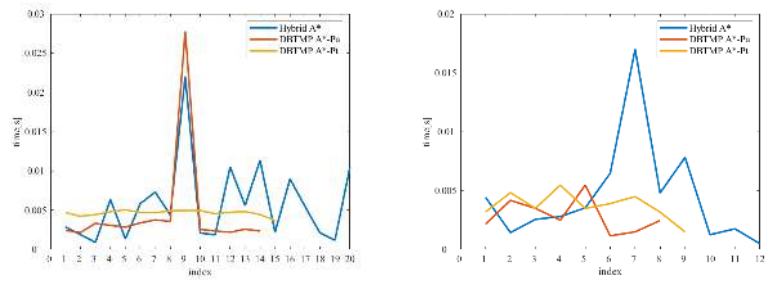

(a) Time-consuming at T_{i} (b) Time-consuming at T_{r}

Figure 15 Time-consuming of single-step extension of motion primitives. The single-step extension time refers to the time required to select the most appropriate MP from the MP library at each MP extension step.

achieve higher efficiency and more reasonable planning results. The experimental conclusions in the real environment are consistent with the simulation.

5 Conclusion

This paper proposed a unified motion planning algorithm framework based on DBTMP generation and selection for heterogeneous vehicle platforms.

(1) An optimized generation method is applied to realize the offline construction of heterogeneous platform MP library. The generated MP library not only distinguishes MPs according to the velocity attributes and platform characteristics but also introduces five types of behavior primitives to expand the types of MPs.

(2) The layered unequal weighted MP online selection framework makes full use of the characteristics of the platform-specific MP library generated offline. Not only the velocity connection relationship of the MP set is limited, but also the selection weight of the single extended behavior primitive and general primitive is distinguished.

(3) The DBTMP A* motion planning algorithm proposed in this paper not only retains the strong environmental adaptability of the original Hybrid A* algorithms but also highlights the characteristic difference between heterogeneous vehicle platforms. Moreover, the proposed method effectively utilizes driving experience to complete the reasonable guidance of the planning results, improving the trajectory smoothness, and significantly reducing the required solution time.

Competing interests

The authors declare that they have no competing interests.

Author's contributions

BW was in charge of the whole trial; HC and JG guided the writing of the manuscript; HG and BW wrote the manuscript; JW and YL assisted with the simulation analyses. All authors read and approved the final manuscript.

Acknowledgements

The work was supported by the National Natural Science Foundation of China (NO.91420203 and NO.61703041).

References

1. Loke, S.W.: Cooperative automated vehicles: a review of opportunities and challenges in socially intelligent vehicles beyond networking. IEEE Transactions on Intelligent Vehicles **4**(4), 509–518 (2019)
2. Wang, S., Zhang, Y., Liao, Z.: Building domain-specific knowledge graph for unmanned combat vehicle decision making under uncertainty. In: 2019 Chinese Automation Congress (CAC), pp. 4718–4721 (2019). IEEE
3. Lin, F., Zhang, Y., Zhao, Y., Yin, G., Zhang, H., Wang, K.: Trajectory tracking of autonomous vehicle with the fusion of dyc and longitudinal–lateral control. Chinese Journal of Mechanical Engineering **32**(1), 16 (2019)
4. Chen, L., Hu, X., Tian, W., Wang, H., Cao, D., Wang, F.-Y.: Parallel planning: a new motion planning framework for autonomous driving. IEEE/CAA Journal of Automatica Sinica **6**(1), 236–246 (2018)
5. Claussmann, L., Revilloud, M., Gruyer, D., Glaser, S.: A review of motion planning for highway autonomous driving. IEEE Transactions on Intelligent Transportation Systems (2019)
6. Katrakazas, C., Quddus, M., Chen, W.-H., Deka, L.: Real-time motion planning methods for autonomous on-road driving: State-of-the-art and future research directions. Transportation Research Part C: Emerging Technologies **60**, 416–442 (2015)
7. Dolgov, D., Thrun, S., Montemerlo, M., Diebel, J.: Path planning for autonomous vehicles in unknown semi-structured environments. The International Journal of Robotics Research **29**(5), 485–501 (2010)
8. Wang, B., Gong, J., Chen, H.: Motion primitives representation, extraction and connection for automated vehicle motion planning applications. IEEE Transactions on Intelligent Transportation Systems (2019)
9. Wang, W., Han, W., Na, X., Gong, J., Xi, J.: A probabilistic approach to measuring driving behavior similarity with driving primitives. IEEE Transactions on Intelligent Vehicles (2019)
10. Taniguchi, T., Nagasaka, S., Hitomi, K., Chandrasiri, N.P., Bando, T., Takenaka, K.: Sequence prediction of driving behavior using double articulation analyzer. IEEE Transactions on Systems, Man, and Cybernetics: Systems **46**(9), 1300–1313 (2015)
11. Bergman, K., Ljungqvist, O., Axehill, D.: Improved path planning by tightly combining lattice-based path planning and optimal control. IEEE Transactions on Intelligent Vehicles (2020)
12. Kammel, S., Ziegler, J., Pitzer, B., Werling, M., Gindele, T., Jagzent, D., Schröder, J., Thuy, M., Goebl, M., Hundelshausen, F.v., *et al.*: Team annieway's autonomous system for the 2007 darpa urban challenge. Journal of Field Robotics **25**(9), 615–639 (2008)
13. Chen, Y.-L., Sundareswaran, V., Anderson, C., Broggi, A., Grisleri, P., Porta, P.P., Zani, P., Beck, J.: Terramax^{TM}: Team oshkosh urban robot. Journal of Field Robotics **25**(10), 841–860 (2008)
14. Urmson, C., Anhalt, J., Bagnell, D., Baker, C., Bittner, R., Clark, M., Dolan, J., Duggins, D., Galatali, T., Geyer, C., *et al.*: Autonomous driving in urban environments: Boss and the urban challenge. Journal of Field Robotics **25**(8), 425–466 (2008)
15. Ferguson, D., Howard, T.M., Likhachev, M.: Motion planning in urban environments. Journal of Field Robotics **25**(11-12), 939–960 (2008)
16. McNaughton, M., Urmson, C., Dolan, J.M., Lee, J.-W.: Motion planning for autonomous driving with a conformal spatiotemporal lattice. In: 2011 IEEE International Conference on Robotics and Automation, pp. 4889–4895 (2011). IEEE
17. Howard, T.M., Green, C.J., Kelly, A., Ferguson, D.: State space sampling of feasible motions for high-performance mobile robot navigation in complex environments. Journal of Field Robotics **25**(6-7), 325–345 (2008)
18. Montemerlo, M., Becker, J., Bhat, S., Dahlkamp, H., Dolgov, D., Ettinger, S., Haehnel, D., Hilden, T., Hoffmann, G., Huhnke, B., *et al.*: Junior: The stanford entry in the urban challenge. Journal of field Robotics **25**(9), 569–597 (2008)
19. Hu, X., Chen, L., Tang, B., Cao, D., He, H.: Dynamic path planning for autonomous driving on various roads with avoidance of static and moving obstacles. Mechanical Systems and Signal Processing **100**, 482–500 (2018)
20. Jiang, Y., Gong, J., Xiong, G., Chen, H.: Research on differential constraints-based planning algorithm for autonomous-driving vehicles. Acta Automatica Sinica **39**(12), 2012–2020 (2013)
21. Yan, J., Qi, W., Jianwei, G., Huiyan, C.: Research on temporal consistency and robustness in local planning of intelligent vehicles. Acta Automatica Sinica **41**(3), 518–527 (2015)
22. Yang, X., Li-Ping, L., Duan-Feng, C., Zi-Cha, H.: Unified modeling of trajectory planning and tracking for unmanned vehicle. Acta Automatica Sinica **45**(4), 799–807 (2019)
23. Cremean, L.B., Foote, T.B., Gillula, J.H., Hines, G.H., Kogan, D., Kriechbaum, K.L., Lamb, J.C., Leibs, J., Lindzey, L., Rasmussen, C.E., *et al.*: Alice: An information-rich autonomous vehicle for high-speed desert navigation. Journal of Field Robotics **23**(9), 777–810 (2006)
24. Ziegler, J., Bender, P., Dang, T., Stiller, C.: Trajectory planning for bertha—a local, continuous method. In: 2014 IEEE Intelligent Vehicles Symposium Proceedings, pp. 450–457 (2014). IEEE
25. Desai, A., Collins, M., Michael, N.: Efficient kinodynamic multi-robot replanning in known workspaces. In: 2019 International Conference on Robotics and Automation (ICRA), pp. 1021–1027 (2019). IEEE
26. Chamzas, C., Shrivastava, A., Kavraki, L.E.: Using local experiences for global motion planning. In: 2019 International Conference on Robotics and Automation (ICRA), pp. 8606–8612 (2019). IEEE
27. Anderson, S.J., Karumanchi, S.B., Iagnemma, K.: Constraint-based planning and control for safe, semi-autonomous operation of vehicles. In: 2012 IEEE Intelligent Vehicles Symposium, pp. 383–388 (2012). IEEE
28. Wang, Q., Wieghardt, C.S., Jiang, Y., Gong, J., Wagner, B.: Generalized path corridor-based local path planning for nonholonomic mobile robot. In: 2015 IEEE 18th International Conference on Intelligent Transportation Systems, pp. 1922–1927 (2015). IEEE
29. Karaman, S., Walter, M.R., Perez, A., Frazzoli, E., Teller, S.: Anytime motion planning using the rrt. In: 2011 IEEE International Conference on Robotics and Automation, pp. 1478–1483 (2011). IEEE
30. Lu, C., Hu, F., Cao, D., Gong, J., Xing, Y., Li, Z.: Transfer learning for driver model adaptation in lane-changing scenarios using manifold alignment. IEEE Transactions on Intelligent Transportation Systems

(2019)
31. Wang, H., Xia, Z., Chen, W.: Lane departure assistance control based on extension combination of steering and braking systems considering human-machine coordination. Journal of Mechanical Engineering **55**(4), 135–147 (2019)
32. Xie, Y., Wei, Z., Zhao, L., Wang, J., Chen, W.: Robust lateral control of intelligent vehicle in the human-machine sharing based on u synthesis. Journal of Mechanical Engineering **56**(4), 104–114 (2020)
33. Guo, C., Kidono, K., Ogawa, M.: Learning-based trajectory generation for intelligent vehicles in urban environment. In: 2016 Ieee Intelligent Vehicles Symposium (iv), pp. 1236–1241 (2016). IEEE
34. Schnelle, S., Wang, J., Su, H., Jagacinski, R.: A driver steering model with personalized desired path generation. IEEE Transactions on Systems, Man, and Cybernetics: Systems **47**(1), 111–120 (2016)
35. Zhao, H., Wang, C., Lin, Y., Guillemard, F., Geronimi, S., Aioun, F.: On-road vehicle trajectory collection and scene-based lane change analysis: Part i. IEEE Transactions on Intelligent Transportation Systems **18**(1), 192–205 (2016)
36. Yao, W., Zeng, Q., Lin, Y., Xu, D., Zhao, H., Guillemard, F., Geronimi, S., Aioun, F.: On-road vehicle trajectory collection and scene-based lane change analysis: Part ii. IEEE Transactions on Intelligent Transportation Systems **18**(1), 206–220 (2016)
37. Xu, D., Ding, Z., Zhao, H., Moze, M., Aioun, F., Guillemard, F.: Naturalistic lane change analysis for human-like trajectory generation. In: 2018 IEEE Intelligent Vehicles Symposium (IV), pp. 1393–1399 (2018). IEEE
38. He, X., Xu, D., Zhao, H., Moze, M., Aioun, F., Guillemard, F.: A human-like trajectory planning method by learning from naturalistic driving data. In: 2018 IEEE Intelligent Vehicles Symposium (IV), pp. 339–346 (2018). IEEE
39. Wächter, A., Biegler, L.T.: On the implementation of an interior-point filter line-search algorithm for large-scale nonlinear programming. Mathematical programming **106**(1), 25–57 (2006)
40. Serban, R., Hindmarsh, A.C.: Cvodes: An ode solver with sensitivity analysis capabilities. Technical report, Technical Report UCRL-JP-200039, Lawrence Livermore National Laboratory (2003)